ROYAL SOCIETY
OF CHEMISTRY

PAPER

Study of the scale-up, formulation, ageing and ammonia adsorption capacity of MIL-100(Fe), Cu-BTC and CPO-27(Ni) for use in respiratory protection filters†

S. Hindocha [ID] and S. Poulston*

The metal–organic frameworks (MOFs) MIL-100(Fe), Cu-BTC and CPO-27(Ni) were synthesised in 1 kg batches. The materials were then formed in two different industrially relevant ways. Firstly, dry granulation was used to produce pellets which were sieved to give material with a 300–1000 μm size, and the fines were subsequently recycled to mimic a large scale industrial process. Secondly, wet granulation with a polymer was used to produce granules which were again sieved to 300–1000 μm. XRD data shows that the structures of MIL-100(Fe) and CPO-27(Ni) remain intact during both forming processes, whilst Cu-BTC is shown to degrade during processing. This is in line with the ammonia adsorption data obtained for the formed materials which evaluated the ammonia adsorption capacity of the materials using breakthrough measurements. MIL-100(Fe) and CPO-27(Ni) are shown to have capacities of 47 mg g^{-1} and 62 mg g^{-1} respectively whilst Cu-BTC has a decreased capacity of 37 mg g^{-1} from 97 mg g^{-1} upon forming. The formed materials were also aged at 25 °C and 80% humidity for a week and the ammonia adsorption capacity re-evaluated. As expected, Cu-BTC decomposed under these conditions, whilst MIL-100(Fe) and CPO-27(Ni) show slightly decreased ammonia adsorption capacities of 36 mg g^{-1} and 60 mg g^{-1} respectively.

Introduction

The National Institute of Occupational Safety and Health (NIOSH) certifies respiratory filters for protection against a wide range of chemical gases, for example ammonia (NH_3), hydrogen sulphide (H_2S) and hydrogen chloride (HCl). Current respiratory protection filters use impregnated activated carbon to provide this broad-spectrum protection. Given the chemical variety of toxic gases it is no surprise that the adsorption performance of activated carbon varies across the gases. Impregnation of a range of inorganic and organic compounds with acidic

Johnson Matthey Technology Centre, Blount's Court Road, Sonning Common, RG4 9NH, UK. E-mail: stephen.poulston@matthey.com
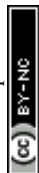
and basic functionality can result in limitations to the effectiveness of the material for individual toxic gas components. Though activated carbon can be optimised for a specific gas, it may not be the most effective means of removing some chemicals.

An alternative approach may be offered by the use of other adsorbent materials specifically targeted at individual gases which can allow for an overall improvement in the filter performance when combined with activated carbon.[1] The use of metal–organic frameworks (MOFs) for the adsorption of toxic gases has been investigated[2,3] due to the tunability of the materials. MOFs provide highly porous structures into which specific functionality can be designed. The selection of metal centres and organic ligands allows materials to be produced with target applications in mind. As a result, MOFs have been investigated for a range of different applications including catalysis,[4] gas storage,[5] gas separations[6] and toxic industrial chemical (TIC) degradation.[7] For example, NU-1000 has been shown to catalytically degrade dimethyl-4-nitrophenyl phosphate.[7] However, more commonly MOFs have been investigated as adsorbents for TIC removal in respiratory protection applications with a range of gases. The adsorption of hydrogen sulphide,[8] chlorine,[9] nitrogen oxide[10] and ammonia[11] into MOF materials have all been studied and generally the incorporation of a specific chemical functionality aids adsorption.

The use of MOFs for the adsorption of ammonia in respiratory protection applications has been investigated in detail. Several reports have systematically investigated different MOFs for ammonia adsorption including the CPO-27/MOF-74 series of materials. This series allows for the investigation of ammonia adsorption onto different vacant metal sites without altering the topology of the MOF.[12] Other reports have used the UiO-66 series of materials to investigate how ligand functionality can impact the MOFs' ammonia adsorption capacity with functionalities that can hydrogen bond to ammonia, increasing material performance.[13]

The forming of MOFs into granules,[14] extrudates[15] and pellets[16] has previously been reported, along with the effect the forming process has on the structure of the MOF and the surface area. The addition of a binder and the amount can also have an impact on the material properties.[17]

This paper aims to investigate three MOFs, MIL-100(Fe), Cu-BTC and CPO-27(Ni), which have been synthesised at a 1 kg scale[18] and formed in industrially relevant processes. These three materials have previously been studied[11] for ammonia adsorption within the literature. Here they have been evaluated for ammonia adsorption capacity using breakthrough measurements, which are compared to an activated carbon currently used within respiratory protection filters. We present the performance of the materials whilst considering the commercial aspects of a respiratory protection product. This included forming the MOF to produce particles with a size range of 300–1000 μm. Testing of the formed materials was completed under conditions appropriate for this application: humid conditions, relevant space velocity and challenge concentrations. The formed samples were aged in conditions comparable to those in the NIOSH specifications to investigate the impact of ageing on the ammonia adsorption performance of the MOFs. NIOSH specifications for respiratory protection devices also detail a drop test and a vibration test, these tests are used to investigate the robustness of the device and the adsorption material. Here we report an attrition test completed on the formed samples to investigate this.

The three materials reported here were selected to investigate the different issues surrounding a respiratory protection product where cost, performance and stability all need to be considered.

Experimental

All materials were purchased from Sigma Aldrich or Alfa Aesar and used as received. Powder X-ray diffraction (XRD) measurements were collected using a Bruker AXS D8 Advance instrument in the parallel beam mode with an Anton Parr HTK1200N sample chamber using Cu K_α radiation at room temperature with a step size of 0.0223° in two theta (2θ) and a 3–100° range. Phase identification was completed using Bruker AXS Diffrac Plus, Eva V19 (1996–2013), Bruker AXS Diffrac Eva V4.0 (2010–2014) software and the ICDD PDF Files: PDF-4+ 2013, COD (REV30738 2011.11.2) database. Crystallite size and lattice parameter measurements were completed using Bruker-AXS Topas 4.2 (1999–2009) software. Nitrogen isotherm measurements were collected on a Quantachrome Autosorb-iQ-MP at 77 K, 2-station model with each station having 1 Torr, 10 Torr and 1000 Torr transducers. MOF samples were degassed using a two-step programme ramp to 90 °C for 2 hours followed by a ramp to 150 °C for 13 hours. All the BET surface areas were calculated using the Rouquerol method.[19,20]

Synthesis of Cu-BTC

$Cu(OH)_2$ and 1,3,5-benzenetricarboxylic acid were stirred in water and MeOH in the following molar ratio (1.5 : 1 : 83 : 175). The resulting mixture was stirred for 48 hours. The resulting bright blue solid was isolated by vacuum filtration, washed with a 1 : 1 water and methanol mixture. The solid was then stirred in MeOH for a further hour, filtered by vacuum filtration, washed with MeOH and dried in ambient conditions.
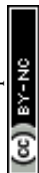
Synthesis of MIL-100(Fe)

$Fe(NO_3)_3 \cdot 9H_2O$ and 1,3,5-benzenetricarboxylic acid were stirred in water in the following molar ratio (1.1 : 1 : 38). The mixture was heated to 90 °C for 18 hours and cooled to room temperature. The red product was isolated using centrifugation (4000 rpm, 20 min) and washed three times in a 1 : 1 water : ethanol mixture before being dried in ambient conditions.

Synthesis of CPO-27(Ni)

$Ni(OH)_2$ and 2,5-dihydroxyterephthalic acid were stirred in water with the following molar ratio (1 : 2 : 98). The resulting mixture was stirred and heated to 90 °C for 18 hours. The resulting dark yellow solid was isolated by vacuum filtration, washed with warm water, and dried at 40 °C overnight.

General procedure for dry granulation

To produce MOF_1 the MOF (2.0 g) was pressed using a 4.5 cm die, considering the force per area the pressure applied to the die was 58.6 MPa. The MOF was pressed for a total of 2 minutes before the resulting pellet was crushed and sieved to give particles with a 300–1000 μm size range.

For the repeated pressing study particles isolated below 300 μm were re-pressed under the above conditions a further five times to afford MOF_2 samples.

General procedure for wet granulation

To produce MOF_3 materials, the MOF (1.0 g) and poly-vinyl alcohol (PVA, 2% by weight) were granulated with water (0.25 ml). The resulting granules were sieved to a 300–1000 μm size range. It is worth noting that it was possible to form granules with the use of little or no binder (<2%), but these tended to be less uniform than those made from a mixture containing a larger amount of binder.

General procedure for the ageing of formed materials

To produce MOF_4 samples, MOF_1 (2 g) was placed in an open container in a humidity controlled chamber at 40 °C and 80% humidity for 7 days. The resulting aged MOF was characterised and tested for ammonia adsorption performance.

General procedure for the attrition test

The MOF (0.2 g) was placed in a small vial which was rolled for 18 hours on a roller mill. The MOF was then sieved to remove all the material below 300 μm and the remaining material weighed.

General procedure for ammonia adsorption test

The formed MOF (∼0.1 g) was placed into a plug flow reactor with an internal diameter of 8 cm, and the reactor bed was packed to a height of 4 mm. A gas stream with a flow rate of 500 ml min^{-1} of ammonia (500 ppm) in nitrogen with 20% oxygen was humidified to an RH of 40%. This stream was passed through the packed bed and analysed using FTIR. The MOF was not pre-treated prior to the experiment.
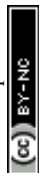
The error within the test was evaluated using a commercial mordenite material and was found to be 4 mg g^{-1}. The ammonia adsorption capacity and break-through times reported here are the average of two experimental runs.

Results and discussion

Each of the materials discussed within this paper is known to adsorb ammonia, however here we discuss various ways to form the three selected MOFs into shapes applicable for respiratory applications.

The MOFs have been granulated in two ways; dry granulation and wet granulation. These two techniques were investigated due to their industrial relevance. The studies completed with MIL-100(Fe), Cu-BTC and CPO-27(Ni) are described here.

Dry granulation is a large scale industrial technique which compacts material and produces non-uniformly shaped pellets. These pellets are then sieved to the application specific size. Material below this size range is recycled to increase the yield of particles in the correct size range. For many materials *i.e.* carbons this repeated compaction has little impact on the performance of the final product, however, it is thought that repeated compaction may have a more significant impact on MOF materials. To determine how dry granulation affects the structure

and the surface area of the MOFs discussed here, materials were pressed and sieved, and the resulting pellets were characterised and tested (MOF_1). The fines (particles < 300 μm) obtained during the sieving step were re-pressed and sieved to the correct size. This process was repeated a total of five times to mimic the large scale industrial process and investigate the how robust the MOF materials were to repeated compaction. Isolated pellets which were pressed a total of five times are noted as MOF_2, and these pellets were characterised and their ammonia adsorption capacity measured.

The secondary forming method investigated was wet granulation, a common industrial process used to produce spherical-like granules. Optimisation of the granulation process to increase the yield of particles in the correct size range is more challenging. Here we report samples made during a small-scale development study. A binding polymer was added to the MOF to produce robust granules. Here we report samples which were produced with the addition of 2% polymer, these are referred to as MOF_3. The granules produced were sieved to the desired particle range prior to characterisation and performance testing.

The ammonia adsorption performance of the shaped MOFs was tested using a plug-flow reactor to obtain breakthrough curves. All breakthrough experiments were completed under humid conditions (40% RH), with a challenge concentration of 500 ppm ammonia. The data obtained was used to calculate the ammonia capacity for each sample. Testing the formed MOFs under these conditions is representative of the NIOSH specifications and gives an indication of how the material would perform in a respiratory protection device.

For a respiratory protection device, there are three types of ageing test within the device specifications: a hot, a cold and a humidity ageing test. Here we report the humidity ageing of the formed MOFs (MOF_4). MOF_1 samples were aged at 25 °C in 80% humidity for 7 days before being fully characterised and tested. We also detail an attrition test which was completed to investigate the robustness of the formed materials. This is an in-house test which has been used to compare the materials to each other. Whilst unlikely to be representative of the NIOSH specification test it has been used to give a qualitative assessment of the material properties.
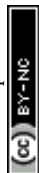
In the following sections the characterisation data and ammonia adsorption capacity of the materials produced is detailed by MOF. Table 1 shows a summary of the sample labels for reference.

CPO-27(Ni)

CPO-27(Ni) was synthesised under aqueous conditions at kilogram scale. Fig. 1 shows the powder XRD pattern for as-synthesised CPO-27(Ni). This is compared to

Table 1 Reference summary of sample names and description

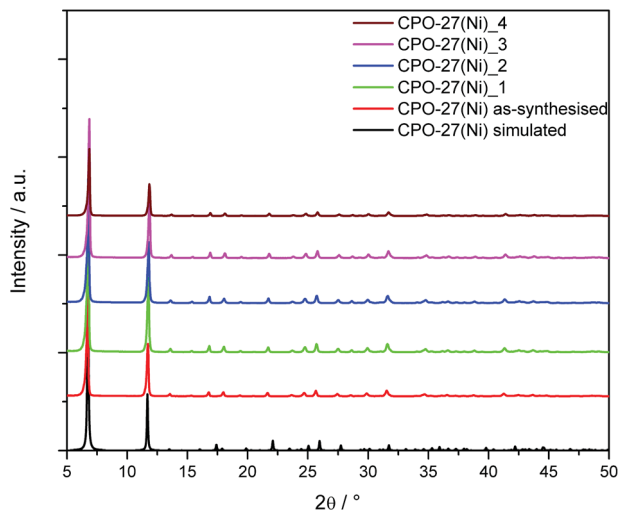| Sample name	Sample description
MOF_1	Dry granulation
MOF_2	Dry granulation repeated 5 times
MOF_3	Wet granulation using 2% polymer
MOF_4	MOF_1 aged at 25 °C, 80% humidity

Fig. 1 Powder X-ray diffraction data of as-synthesised CPO-27(Ni) compared to the formed and aged samples; the calculated pattern of CPO-27(Ni) was simulated from the crystal structure.
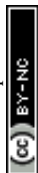
the powder pattern simulated from the crystal structure and the XRD patterns of the formed samples.

Rietveld refinement of the as-synthesised material shows the sample to be phase pure CPO-27(Ni). The XRD patterns of CPO-27(Ni)_1 and CPO-27(Ni)_2 show that the structure is retained, indicating that repeated compaction during dry granulation has little impact on the structure of CPO-27(Ni). The crystal structure is also retained for the wet granulated material (CPO-27(Ni)_3) and the aged sample (CPO-27(Ni)_4).

Whilst the XRD data suggests there is little change in the structure of the MOF, the calculated BET surface area shows larger variation between the samples (Table 2). The surface area measurements show that the compaction of the as-synthesised CPO-27(Ni) causes a decrease in surface area. As the sample is repeatedly compacted the surface area continues to decrease (CPO-27(Ni)_2). This is not unexpected and has been previously reported by Peterson *et al.*[21] Interestingly, the sample which had been wet granulated (CPO-27(Ni)_3) showed an

Table 2 Lattice parameters and crystallite size calculated from the Rietveld refinement of the powder XRD data from the CPO-27(Ni) series of materials along with the BET surface area

Sample ID	a (Å)	c (Å)	Crystallite size (nm)	BET surface area (m^2 g^{-1})
CPO-27(Ni)_as-synthesised	25.9636(3)	6.69534(12)	82.0(15)	937
CPO-27(Ni)_1	25.9469(5)	6.68919(2)	73.1(14)	855
CPO-27(Ni)_2	25.9525(15)	6.68914(5)	76.2(17)	805
CPO-27(Ni)_3	25.9583(3)	6.6912(4)	89.4(16)	1319
CPO-27(Ni)_4	25.9504(12)	6.6897(6)	85.0(2)	257

increased surface area. Currently the reason for this is unclear and work is ongoing to investigate this further. The aged sample, CPO-27(Ni)_4, shows the lowest surface area measured, suggesting there is some decomposition of the material during humidity ageing which is not observable in the powder XRD data.

The ammonia adsorption capacity of the formed materials was evaluated. Fig. 2 shows the breakthrough curves for the CPO-27(Ni) samples. Notably the as-synthesised powder sample was not tested due to back pressure issues encountered. The breakthrough curves were used to calculate the ammonia adsorption capacity of each sample and identify the breakthrough time at 12.5 ppm ammonia. These are shown in Table 3.

The breakthrough time has been recorded at 12.5 ppm as this is the ammonia limit set within NIOSH specifications for respiratory protection devices. An activated carbon sample was also tested so that the results obtained could be compared to a control sample. The breakthrough curves show that the CPO-27(Ni) samples have a significantly increased ammonia capacity and breakthrough concentration time over the activated carbon sample.

The ammonia adsorption capacity (Table 3) of the wet granulated sample CPO-27(Ni)_3 is lower than that of the dry granulated samples (CPO-27(Ni)_1 and CPO-27(Ni)_2). Whilst the ammonia capacity of CPO-27(Ni)_2 is comparable to CPO-27(Ni)_1, the breakthrough time is reduced. This is also observed for the aged sample CPO-27(Ni)_4, although the ammonia capacity is comparable to the unaged sample CPO-27(Ni)_1 the breakthrough time is more than halved. It is of note that the shape of the breakthrough curve for CPO-27(Ni)_4 is different to CPO-27(Ni)_1, indicating that the kinetics of adsorption have changed and that much of the ammonia capacity is in the high concentration ammonia region. This is also the case for CPO-27(Ni)_2. For respiratory protection devices, having additional capacity within this region is not ideal as it is not utilised.

The data obtained from the attrition test shows that, as expected, repeated compaction produces more robust granules, exemplified by CPO-27(Ni)_2. It can
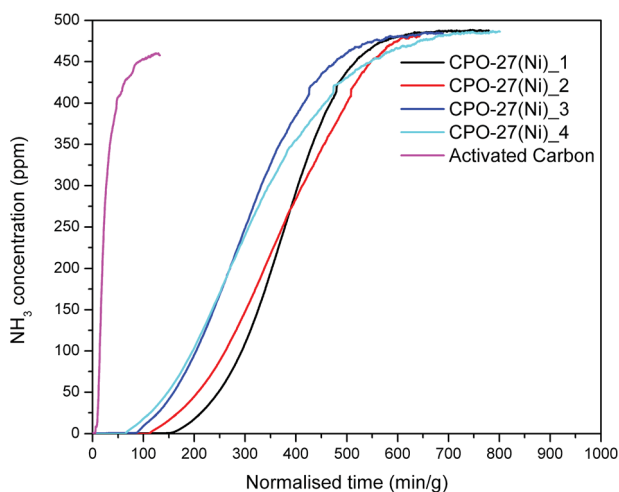

Fig. 2 Ammonia breakthrough curves for CPO-27(Ni)_1 to CPO-27(Ni)_4 and a commercial activated carbon sample.
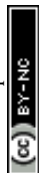
Table 3 Ammonia adsorption capacity of CPO-27(Ni) materials and the breakthrough time at 12.5 ppm ammonia

Sample	Ammonia adsorption capacity (mg g^{-1})	Breakthrough time (min g^{-1})	Attrition test percentage loss (%)
Activated carbon	8	9	0
CPO-27(Ni)_1	64	189	29
CPO-27(Ni)_2	65	141	3
CPO-27(Ni)_3	51	106	18
CPO-27(Ni)_4	61	90	64

also be seen that the use of a binder in CPO-27(Ni)_3 has a positive impact on the robustness of the granules when compared to CPO-27(Ni)_1. The aged material CPO-27(Ni)_4 is shown to have a large percentage loss suggesting that whilst ageing the material may not have a large impact on the ammonia capacity, the strength of the granules is adversely impacted.
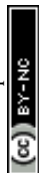
Further work to improve the robustness of the CPO-27(Ni) granules is ongoing, however the data presented here shows the increased ammonia adsorption capacity of CPO-27(Ni) when compared to activated carbon.

MIL-100(Fe)

MIL-100(Fe) was synthesised under aqueous conditions and washed with a 1 : 1 ethanol/water mixture. The main issue encountered during the scale-up synthesis is the isolation of the product. Vacuum filtration of the material is slow due to the small particle size produced. A study investigating flocculation of the material was completed, however this proved unsuccessful. Due to the slow filtration, the final product was isolated by centrifugation. Fig. 3 shows the measured powder XRD data for the as-synthesised MIL-100(Fe) compared to the simulated powder pattern. Rietveld refinement of the powder pattern shows the material to be phase pure MIL-100(Fe). The formed samples are also shown to be phase pure MIL-100(Fe) as is the aged material, MIL-100(Fe)_4.

As-synthesised MIL-100(Fe) has a BET surface area of 1212 m^2 g^{-1}, comparable to literature values.[22] Table 4 shows the surface area values for the MIL-100(Fe) materials. Forming MIL-100(Fe) using dry granulation (MIL-100(Fe)_1 and MIL-100(Fe)_2) results in a decrease in surface area, as seen with CPO-27(Ni). MIL-100(Fe)_4 also shows a decrease in surface area when compared to MIL-100(Fe)_1, indicating that humidity ageing of the material does have an impact on the material despite powder XRD data showing that MIL-100(Fe)_4 is phase pure. Addition of the polymer for wet granulation is shown to have little impact on the surface area of MIL-100(Fe)_3, unlike the wet granulated CPO-27(Ni).

Table 5 shows the ammonia adsorption capacity and breakthrough time at 12.5 ppm ammonia for the formed MIL-100(Fe) samples. The dry granulated sample MIL-100(Fe)_2 has a lower ammonia capacity and a shorter breakthrough time than MIL-100(Fe)_1, showing that repeated compaction of the material has an impact on the performance. MIL-100(Fe)_4 shows a larger decrease in both the capacity and breakthrough time, indicating the adverse effect of ageing the MOF under humid conditions. The wet granulated sample MIL-100(Fe)_3 shows
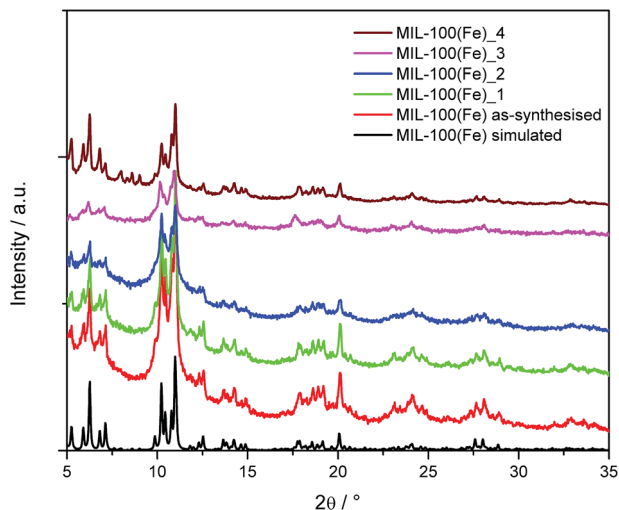
Fig. 3 Powder X-ray diffraction data of as-synthesised MIL-100(Fe) compared to the formed and aged samples; the calculated pattern of MIL-100(Fe) was simulated from the crystal structure.

Table 4 Lattice parameters and crystallite size calculated from the Rietveld refinement of the powder XRD data from the MIL-100(Fe) series of materials along with the BET surface area

Sample ID	a (Å)	Crystallite size (nm)	BET surface area ($m^2 \ g^{-1}$)
MIL-100(Fe) as-synthesised	73.1389(7)	50.29(1)	1212
MIL-100(Fe)_1	73.1616(13)	65.32(5)	928
MIL-100(Fe)_2	73.1120(12)	35.45(36)	522
MIL-100(Fe)_3	72.9992(41)	21.21(80)	1172
MIL-100(Fe)_4	73.17658(41)	81.22(1)	727

a slightly increased ammonia capacity when compared to MIL-100(Fe)_1, however, when the error within the test is considered the difference in the data is small, suggesting the addition of the polymer has a negligible impact on the MOF.

The attrition test data shows all the formed samples produced to be relatively robust. However, as with CPO-27(Ni)_4 the aged sample MIL-100(Fe)_4 shows an increased mass loss compared with the other materials. Humidity ageing was completed on the dry granulated MIL-100(Fe)_1, and work is currently underway to study the ageing effects on the wet granulated material.

Cu-BTC

Cu-BTC was synthesised in a water/methanol solvent mixture and washed with methanol. It is of note that washing the material with water alone results in a different material which was not identified. Fig. 4 shows the measured XRD patterns for the Cu-BTC samples. As-synthesised Cu-BTC was activated at 120 °C
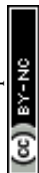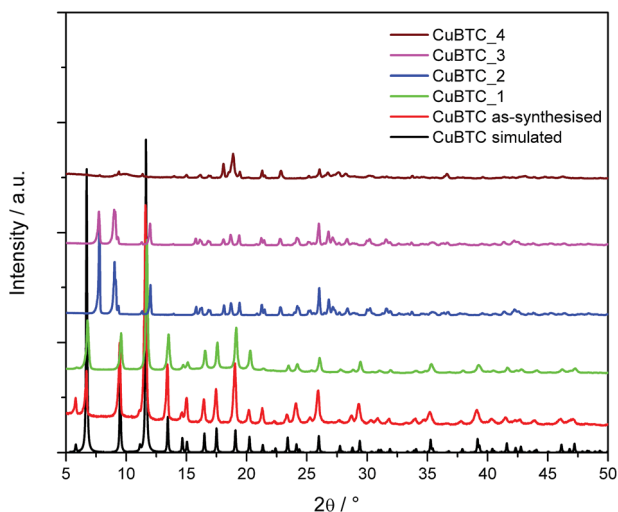
Table 5 Ammonia adsorption capacity of MIL-100(Fe) materials and the breakthrough time at 12.5 ppm ammonia

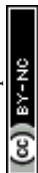| Sample	Ammonia adsorption capacity (mg g^{-1})	Breakthrough time (min g^{-1})	Attrition test percentage loss (%)
MIL-100(Fe)_1	47	135	3
MIL-100(Fe)_2	44	92	8
MIL-100(Fe)_3	50	100	2
MIL-100(Fe)_4	36	32	74

Fig. 4 Powder X-ray diffraction data of as-synthesised Cu-BTC compared to the formed and aged samples; the calculated pattern of Cu-BTC was simulated from the crystal structure.

under vacuum and subsequently hydrated by exposure to the ambient atmosphere prior to forming.

The XRD patterns of the formed samples show that only Cu-BTC_1 retains the Cu-BTC structure, this was confirmed by the Rietveld refinement. Repeated compaction of the fines produced Cu-BTC_2, and the XRD data shows that this has caused the structure to decompose. This decomposition can also be observed in the colour of the material. Fig. 5 shows an image of the dry granulated Cu-BTC pellets; after each cycle of compaction the colour of the sample changes.

Using the powder XRD patterns of Cu-BTC_2, _3 and _4, phase identification of the samples was attempted; this showed that the materials consist of a mixed phase system, containing hydrogen triaquabenzene-1,3,5-tricarboxylate copper(II) along with a second decomposition product. To the best of our knowledge the identity of the Cu-BTC decomposition product has not yet been identified in the literature.

Table 6 shows the BET surface area of the Cu-BTC samples. Whilst the initial compaction results in a slight loss of surface area, the decomposition of the Cu-BTC structure causes a larger decrease in the BET surface area, which is observed
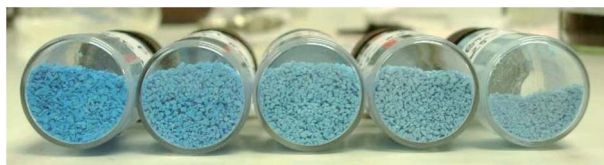
Fig. 5 Cu-BTC_1 (far left) and Cu-BTC_2 (far right).

Table 6 Phase ID, lattice parameters and crystallite size calculated from the Rietveld refinement of the powder XRD data from the Cu-BTC series of materials along with the BET surface area

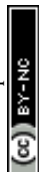| Sample ID	Phase ID	a (Å)	Crystallite size (nm)	BET surface area (m^2 g^{-1})
Cu-BTC as-synthesised	Cu-BTC	26.3876(19)	57.0(2)	1605
Cu-BTC_1	Cu-BTC	26.3629(10)	49.6(2)	924
Cu-BTC_2	Mixed phase system	N/A	N/A	144
Cu-BTC_3	Mixed phase system	N/A	N/A	147
Cu-BTC_4	Mixed phase system	N/A	N/A	132

for Cu-BTC_2. Wet granulation of Cu-BTC (Cu-BTC_3) and ageing of the material (Cu-BTC_4) results in the same decomposed structure and loss of surface area.

The change in structure also results in a decrease in the ammonia adsorption capacity and breakthrough time, shown in Table 7. The ammonia adsorption capacity of Cu-BTC_1 is, as expected, the highest of all the materials reported within this paper. Repeated compaction of Cu-BTC results in a decrease in capacity and breakthrough time, exemplified by Cu-BTC_2. Cu-BTC_4 shows a decreased ammonia adsorption capacity and a much-reduced breakthrough time when compared to Cu-BTC_1, showing the impact ageing the material in humid conditions has on the performance.

The attrition test shows that decomposition of Cu-BTC during repeated compaction does not have a massive impact on the robustness of the granules, with an 18% loss for Cu-BTC_1 and a 17% loss for Cu-BTC_2. This contrasts with the aged material Cu-BTC_4 which decomposed during the ageing test and has a much larger percentage loss. Interestingly, part of this loss was due to oversized granules >1000 μm, indicating that some granules had agglomerated.

Table 7 Ammonia adsorption capacity of Cu-BTC materials and the breakthrough time at 12.5 ppm ammonia

Sample	Ammonia adsorption capacity (mg g^{-1})	Breakthrough time (min g^{-1})	Attrition test percentage loss (%)
Cu-BTC_1	105	210	18
Cu-BTC_2	38	47	17
Cu-BTC_3	19	43	11
Cu-BTC_4	46	80	69

The change in structure and subsequent reduced ammonia adsorption performance of Cu-BTC upon granulation and ageing suggests that the material may not be robust enough for respiratory protection devices.

Conclusions

Three MOFs have been synthesised at a 1 kilogram scale and the resulting products have been formed *via* wet and dry granulation routes. The materials have been shown to produce pellets and granules using different industrially relevant processes. The formed materials were subsequently tested for ammonia adsorption using breakthrough measurements.

CPO-27(Ni) is shown to have good ammonia adsorption capacity in both dry and wet granulated forms. The data shows that wet granulated samples have a lower capacity than the dry granulated materials, indicating that in this case compaction may be the preferred method of forming for this MOF. Ageing the sample has little impact on the ammonia capacity of the material although it does decease the breakthrough time, and from the shape of the breakthrough curve it can be seen that the kinetics of adsorption change.
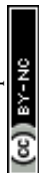
MIL-100(Fe) is shown to have the lowest fresh ammonia adsorption capacity of the three MOFs investigated here. Repeated dry granulation has a small impact on the capacity of the MOF but a larger impact on the breakthrough time when compared to MIL-100(Fe)_1. It is interesting that wet granulation with 2% polymer (MIL-100(Fe)_3) produces granules which have both a good ammonia adsorption capacity and breakthrough time. Ageing MIL-100(Fe) results in a small decrease in capacity and a large decrease in breakthrough time, this again is due to a change in the kinetics of adsorption.

It has been shown that Cu-BTC can be granulated using dry granulation, however repeated dry granulation, completed to reduce waste, results in decomposition of the MOF. Cu-BTC_1 has been shown to have the highest fresh ammonia adsorption capacity of the three MOFs reported here. However, ageing of the sample results in a significant change in the structure and a decrease in ammonia capacity. In the data presented here it has not been possible to form Cu-BTC in the industrially relevant ways investigated whilst retaining high ammonia adsorption capacities. Forming Cu-BTC in relevant conditions and investigating the resulting stability of the material requires further work.

The data presented here indicates that overall CPO-27(Ni) is the preferred MOF for use in the adsorption of ammonia within respiratory protection devices. However, each of the MOFs reported here has drawbacks: Cu-BTC has stability problems during forming, MIL-100(Fe) has a lower performance compared to both CPO-27(Ni) and Cu-BTC, and CPO-27(Ni) is costly to synthesise. These three material properties, stability, performance and cost, all need to be considered when producing a respiratory protection device.

Acknowledgements

References

1 B. GmbH, *US Pat.*, 0 166 970, 2016.
2 J. B. DeCoste and G. W. Peterson, *Chem. Rev.*, 2014, **114**, 5695.
3 G. W. Peterson, D. K. Britt, D. T. Sun, J. J. Mahle, M. Browe, T. Demasky, S. Smith, A. Jenkins and J. A. Rossin, *Ind. Eng. Chem. Res.*, 2015, **54**, 3626.
4 E. D. Metzger, C. K. Brozek, R. J. Comito and M. Dincă, *ACS Cent. Sci.*, 2016, **2**, 148.
5 J. Jiang, H. Furukawa, Y.-B. Zhang and O. M. Yaghi, *J. Am. Chem. Soc.*, 2016, **138**, 10244.
6 D.-L. Chen, H. Shang, W. Zhu and R. Krishna, *Chem. Eng. Sci.*, 2014, **117**, 407.
7 J. E. Mondloch, M. J. Katz, W. C. Isley III, P. Ghosh, P. Liao, W. Bury, G. W. Wagner, M. G. Hall, J. B. DeCoste, G. W. Peterson, R. Q. Snurr, C. J. Cramer, J. T. Hupp and O. K. Farha, *Nat. Mater.*, 2015, **14**, 512.
8 L. Hamon, C. Serre, T. Devic, T. Loiseau, F. Millange, G. Feréy and G. De Weireld, *J. Am. Chem. Soc.*, 2009, **131**, 8775.
9 J. B. DeCoste, M. A. Browe, G. W. Wagner, J. A. Rossin and G. W. Peterson, *Chem. Commun.*, 2015, **51**, 12474.
10 A. M. Ebrahim, B. Levasseur and T. J. Bandosz, *Langmuir*, 2013, **29**, 168.
11 M. J. Katz, A. J. Howarth, P. Z. Moghadam, J. B. DeCoste, R. Q. Snurr, J. T. Hupp and O. K. Farha, *Dalton Trans.*, 2016, **45**, 4150.
12 T. G. Glover, G. W. Peterson, B. J. Schindler, D. Britt and O. Yaghi, *Chem. Eng. Sci.*, 2011, **66**, 163.
13 H. Jasuja, G. W. Peterson, J. B. DeCoste, M. A. Browe and K. S. Walton, *Chem. Eng. Sci.*, 2015, **124**, 118.
14 P.-J. Kim, Y.-W. You, H. Park, J.-S. Chang, Y.-S. Bae, C.-H. Lee and J.-K. Suh, *Chem. Eng. J.*, 2015, **262**, 683.
15 D. Crawford, J. Casaban, R. Haydon, N. Giri, T. McNally and S. L. James, *Chem. Sci.*, 2015, **6**, 1645.
16 V. Finsy, L. Ma, L. Alaerts, D. E. De Vos, G. V. Baron and J. F. M. Denayer, *Microporous Mesoporous Mater.*, 2009, **120**, 221.
17 C. A. Grande, V. I. Águeda, A. Spjelkavik and R. Blom, *Chem. Eng. Sci.*, 2015, **124**, 154.
18 P. L. C. Johnson Matthey, *WO Pat.*, 160683, 2013.
19 J. Rouquerol, P. Llewellyn and F. Rouquerol, *Stud. Surf. Sci. Catal.*, 2007, **160**, 49.
20 K. S. Walton and R. Q. Snurr, *J. Am. Chem. Soc.*, 2007, **129**, 8552.
21 G. W. Peterson, J. B. DeCoste, F. Fatollahi-Fard and D. K. Britt, *Ind. Eng. Chem. Res.*, 2014, **53**, 701.
22 Y.-K. Seo, J. W. Yoon, J. S. Lee, U.-H. Lee, Y. K. Hwang, C.-H. Jun, P. Horcajada, C. Serre and J.-S. Change, *Microporous Mesoporous Mater.*, 2012, **157**, 137.